Computational modeling of solid tumor growth: the avascular stage

Didier Bresch [a] Thierry Colin [b] Emmanuel Grenier [c]
Benjamin Ribba [d] Olivier Saut [e]

[a] *Lama, Université de Savoie, CNRS UMR 5127, Campus scientifique, 73376 Le Bourget du lac cedex, France*

[b] *Université Bordeaux 1, Institut de Mathématiques, INRIA Futurs-MC2, 351 cours de la libération, 33405 Talence Cedex, France*

[c] *Unité de Mathématiques Pures et Appliquées, CNRS UMR 5669, Ecole Normale Supérieure de Lyon, 69364 Lyon cedex 07, France*

[d] *Université de Lyon, Lyon, F-69003, France; Université Lyon 1, Ciblage Thérapeutique en Oncologie (EA3738), Faculté de Médecine Lyon-Sud, Oullins, F-69921, France*

[e] *Université Bordeaux 1, Institut de Mathématiques, CNRS UMR 5254 and INRIA Futurs-MC2, 351 cours de la libération, 33405 Talence Cedex, France*

Abstract

In this paper, we present a mathematical model for avascular tumor growth and its numerical study in two and three dimensions. For this purpose, we use a multiscale model using PDEs to describe the evolution of the tumor cell densities. In our model, cell cycle regulation depends mainly on micro-environment. The cancer growth of volume induces cells motion and tumor expansion. According to biology, cells grow against a basal membrane which interacts mechanistically with the tumor. We use a level set method to describe this membrane and we compute its influence on cell movement thanks to a Stokes equation. The evolution of oxygen, diffusing from blood vessel to cancer cells and used to estimate hypoxia, is given by a stationary diffusion equation solved with a penalization method. The model has been applied to investigate the therapeutic benefit of anti-invasive agents and constitutes now the basis of a numerical platform for tumor growth simulation.

Key words: Avascular tumor growth. Multiscale models. Cell cycle modeling. Fluid dynamics. Level-set methods.

Email addresses: Didier.Bresch@univ-savoie.fr (Didier Bresch), Thierry.Colin@math.u-bordeaux1.fr (Thierry Colin),

1 Introduction

Small tumors appear when epithelial cells lack of growth control. Uncontrolled proliferation can be the result of different alterations of normal cells properties (see [1] for a review). In particular, disruption of cell cycle can lead cells to proliferate without limitation leading to the formation of an initial tumor nodule.

To proliferate, cells need nutrients and oxygen coming from existing vascular vessels surrounding the tissue where the tumor growth. It is generally admitted that the process of cancer growth can be divided into two stages. The first stage is the avascular stage where the cells receive nutrient and oxygen from existing blood vasculature. Avascular tumors can grow until the lack of nutrient and oxygen limits the extension of the initial nodule. Generally, it is admitted that an avascular tumor can not grow over 10^6 cells. Starving cells have the ability to secrete vessel chemoattractants in order to induce the formation of new blood vessels towards the tumor. This is called the process of angiogenesis [2]. When a tumor is able to induce angiogenesis, it can become vascularized. Vascular tumor are much less limited in terms of nutrient and oxygen and can metastasize to distant organs through cells penetration in the newly formed blood vessels.

In this paper, we will focus on the avascular stage where the regulation of the cell cycle is among the most important factors. It is known that the progression in the cell cycle is conditioned by the tumor microenvironment. If the environment conditions are not adequate (*e.g.* lack of nutrient) the progression is stopped and the division process ceases [2,3]. Furthermore, it is quite clear that the macroscopic aspects, mechanical constrains and tissue deformation plays a significant role in tumor growth and therefore, there should be complex interaction between the macroscopic level (tissue level) and the cell cycle regulation (cell level).

There is a significant number of mathematical models representing tumor growth though the regulation of cell cycle and the macroscopic and tissue level. However, these two factors are somehow separated. Indeed, macroscopic models of tumor growth integrating tissue mechanical constraints generally do not integrate precisely molecular or cellular events occurring during cell cycle regulation.

The present highly integrated framework has been initiated in [5], where moreover, genetic level was taken into account. In [6], we showed the significant

Emmanuel.Grenier@umpa.ens-lyon.fr (Emmanuel Grenier),
Benjamin.Ribba@recherche.univ-lyon1.fr (Benjamin Ribba),
Olivier.Saut@math.u-bordeaux1.fr (Olivier Saut).

potential of this approach to investigate recent therapeutic developments.

Here, we describe with more details the mathematical and computational model which will constitute the basis for further therapeutic investigations through successive biological components integration.

The model is a multiscale model based on a set of PDEs to describe avascular growth. The tumor will be described by the densities of cells (or numbers of cell per volume unit) in the quiescent and proliferating phases evolving in time and age in the cell cycle (the set of mutations a cell has to undergo in order to divide). Hence, these densities are governed by equations with an advection term in space (corresponding to the movement created by the cellular division) and an aging term as the cells progress in the cell cycle. The transition between phases and cellular division will be accounted through the boundary conditions in these equations.

The transition between quiescent and proliferating phases is controlled by environmental regulation signals. Our model takes into account two signals influencing cancer growth. The first one, *overpopulation*, is activated when there is not enough free space for cells to proliferate. The second one, *hypoxia*, is due to the lack of oxygen. Both signals have been shown to play a significant role in tumor growth [2,3].

In the model, tumor cells are surrounded by a basal membrane. This membrane may slow the cancer growth. To describe the mechanical force of the membrane on the tumor, we use the immersed interface boundary method [7], where the membrane is represented by a level set function [8]. From this level set function, we compute the elastic force adapting a method from Cottet and Maître [9]. This force appears as a source term in the Stokes equations that we use to compute the velocity and pressure. In the vicinity of the membrane, cancer cells release matrix metalloproteinases (MMP), which are enzymes able to degrade the components of the basal membrane.

This paper is organized as follows. In Section 1, we present our model. In Section 2, we present the numerical schemes used to discretize this model. Finally, in Section 3, we perform various numerical experimentations.

2 Description of the model

In the following, we are interested in the experimental setup described in Figure 1. We consider the case of a growing cluster of cancer cells in a square domain containing a source of oxygen and a basal membrane.

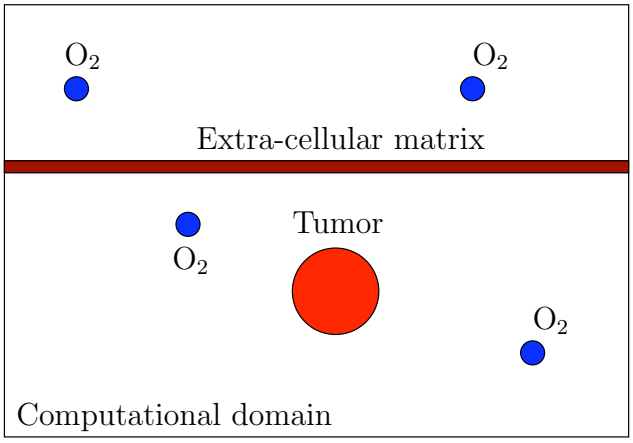

Fig. 1. Experimental setup considered in this paper.

2.1 Cellular description

Two different cell densities will be considered as tumor cells can be in two states. The proliferating one where cells divide and leads to the tumor growth. And according to our hypothesis, if the environmental conditions are unfavorable, cells turns to a quiescent state, in which cellular division no longer occurs. We considered that a cell can stay in a quiescent state forever. However, if the environment changes to be favorable again, cells can turn back into the proliferating state. The environmental conditions are checked at one point in the cell cycle: the *restriction point* [10].

The mathematical description is done through an age-structured model of the cell cycle. Cells evolve with respect to time t and to age a. We use a simplified model with two proliferating phases (whose densities are denoted by P_1 and P_2) and one quiescent phase (denoted by Q). Note that the variables P_1 and P_2 depend on time, space and age (t, x, y, z, a) while Q only depends on time and space (t, x, y, z) (since we assume that cells do not evolve in age in the quiescent phase). The cycle is summarized in Figure 2. The durations of the phases P_1 and P_2 are denoted by $a_{\max,P_1}$ and $a_{\max,P_2}$ respectively. They can be evaluted from the literature [11,12].

2.2 Environmental conditions

In the model, two factors regulates cell cycle transitions. The first one is related to the total cell density. If this density is above a particular threshold, we consider that proliferating cells become quiescent. The second one is the

Fig. 2. Principle of the simplified cell cycle considered in this paper. The transition between phases P_1 and P_2 is controlled by the boolean function f at the restriction point.

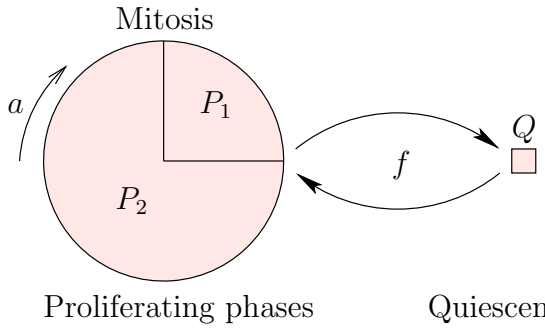

oxygen concentration. As before, if this concentration is below a particular threshold, we consider that proliferating cells become quiescent. Therefore, at each point of the computational domain, we compute the number of cell and the quantity of oxygen that is available.

In order to describe these tests quantitatively we introduce the following boolean function

$$f(t,x,y,z) = \begin{cases} 1 \text{ if } \int_0^{a_{\max,P_1}} P_1(t,x,y,z,a)da + 2\int_0^{a_{\max,P_2}} P_2(t,x,y,z,a)da \\ \quad +Q(t,x,y,z) < \tau_o \text{ and } C(t,x,y,z) > \tau_h, \\ \\ 0 \text{ otherwise,} \end{cases} \tag{1}$$

where τ_o is the cancer overpopulation threshold, τ_h the hypoxia threshold. Here $C(t,x,y,z)$ denotes the concentration of oxygen at point (x,y,z) (see the equation (7) below). The factor 2 before the population of phase P_2 comes from the fact that the cells present in the second part of the cycle will divide and therefore contribute to the increase of volume.

The evolution of the population of cells in the cycle is described by

$$\begin{cases} \partial_t P_1 + \partial_a P_1 + \nabla\cdot(\mathbf{v}_{P_1} P_1) = 0, \\ \partial_t P_2 + \partial_a P_2 + \nabla\cdot(\mathbf{v}_{P_2} P_2) = 0, \\ \partial_t Q + \nabla\cdot(\mathbf{v}_Q Q) = (1-f)P_1(a = a_{\max,P_1}) - \left[\frac{d}{dt}f\right]^+ Q(t^-), \end{cases} \tag{2}$$

where $\mathbf{v}_{P_1}$, $\mathbf{v}_{P_2}$, $\mathbf{v}_Q$ are the velocities of the three phases P_1, P_2 and Q respectively, which we shall determine later on. We have denoted by $\left[\frac{d}{dt}f\right]^+$ the positive part of $\left[\frac{d}{dt}f\right]$. According to the third equation of (2), if the environment is not favorable, *i.e.* $f = 0$, cells in the phase P_1 become quiescent and appear as a source term in the equation driving the evolution of the phase Q.

If the environment is appropriate, *i.e.* $f = 1$, these cells enter the phase P_2. If the environment has just turned to be favorable, the quiescent cells reenter a mitotic phase (P_2) and leave the quiescent phase. This transition is captured by the Dirac mass $\left[\frac{d}{dt}f\right]^+$.

To describe the transition between the cycle phases and the cell division, we write the following boundary conditions on the age a:

$$\begin{cases} P_1(a=0) = 2\,P_2(a=a_{\max,P_2}), \\ \\ P_2(a=0) = f\,P_1(a=a_{\max,P_1}) + \left[\frac{d}{dt}f\right]^+ Q(t^-). \end{cases} \tag{3}$$

The first equation of (3) corresponds to the cell division. The second one states that:

- If the environment is appropriate, the cells in the first age of the P_2 phase are cells previously in the last age of P_1.
- If the conditions change to be favorable, cells in the quiescent phase Q are added to the phase P_2 through the term $\left[\frac{d}{dt}f\right]^+ Q$.

Remark 1 *As the cells do not evolve in age in the quiescent phases, the boundary conditions on Q appear as a source term in Eq. (2).*

We also denote by M the density of normal cells or healthy tissue. This density evolve through an advection equation

$$\partial_t M + \mathbf{v}_M \cdot \nabla M = 0. \tag{4}$$

We will also assume that the total number of cells per unit volume is constant. Hence the following saturation assumption holds

$$M + Q + \int_0^{a_{\max,P_1}} P_1(a)da + \int_0^{a_{\max,P_2}} P_2(a)da = N_0, \tag{5}$$

meaning that the space is occupied by tumor cells or non-cancerous tissue where N_0 denotes the (constant) total number of cell per unit volume. Due to this condition, the density M can be directly obtained from the tumoral density and thus Eq. (4) will not be explicitly solved.

Since the system is mainly driven by the birth of new cells in the domain, we assume that the cells undergo a passive transport and move at the velocity of a "surrounding" fluid $\mathbf{v}$. We therefore take $\mathbf{v}_{P_1} = \mathbf{v}_{P_2} = \mathbf{v}_Q = \mathbf{v}_M$ in (2) and (4).

Let us now derive Eq. (5) w.r.t. time and use equations (2), (4) and the

boundary conditions (3). It is straightforward to see that it leads to a condition on the velocity $\mathbf{v}$ namely

$$\nabla \cdot \mathbf{v} = \frac{1}{N_0} P_2(a_{\max,P_2}). \tag{6}$$

The divergence of the velocity field is non negative. This corresponds to an increase of the volume of the tissue and will create a movement of the cells from the center of the domain to the boundary. The healthy cells are therefore "pushed out" through the boundary.

To determine the velocity $\mathbf{v}$, we need an additional equation on $\mathbf{v}$ to close the system (see section 2.4).

2.3 Distribution of oxygen

According to our model hypothesis, oxygen is essential to the division of cells. We shall describe its distribution at the point (x, y, z) and time t by its concentration $C(t, x, y, z)$. The oxygen undergoes a diffusion process and is consumed by tumors cells in proliferating phases, *i.e.* we neglect consumption of the quiescent state. As oxygen molecules are much smaller than cells, they are not affected by the motion created by the mitosis.

We assume that in a part O of the computational domain Ω, this concentration is fixed. One can imagine O being a network of blood vessel for instance.

We also make the adiabatic approximation : the diffusion process occurs on much smaller time scales that the cellular division. Therefore we suppose that the equilibrium is reached instantaneously. Collecting these assumptions yields the following elliptic equation on C

$$\begin{cases} -\nabla \cdot (K \nabla C) = -\alpha \sum_{i=1,2} \int_0^{a_{\max,P_i}} P_i(a) da, \\ C = C_0 \ \text{ on } \ \partial\Omega, \\ C = C_{\max} \ \text{ on } \ \mathrm{O}, \end{cases} \tag{7}$$

where α is the rate of consumption by the proliferating cells and K is the coefficient of diffusion. We assumed this function K to be dependent on cells distributions and basal membrane. This function is fully described in the appendix A.

2.4 Computation of the velocity

To determine the dynamic of the motion of the tumor, we have to compute the hydrodynamic variables namely the velocity $\mathbf{v}$ and the pressure P. Classically, they are obtained through a Darcy's law [6,13]. However, aside from porous media, this law is no longer relevant in three dimensions of space (2D Darcy's law can be derived from the 3D Navier-Stokes equations for a shallow flow between two plates [14]). In this paper we chose to use the Stokes system to describe the hydrodynamical variables:

$$-\nabla \cdot (\nu D(\mathbf{v})) + \nabla \left(P + \frac{2}{d} \nu \mathrm{tr}(D(\mathbf{v})) \right) = \mathbf{F}, \tag{8}$$

where $D(v)_{ij} = (\partial_j v_i + \partial_i v_j)$ is the deformation rate tensor, ν the viscosity (which will depend linearly on the tumor density in the sequel, see appendix A), $\mathbf{F}$ the force due to the membrane [7] and $d(= 2, 3)$ the dimension of space. This elastic force $\mathbf{F}$ is vanishing outside the membrane.

From (6), we know that the total number of cells is constant in the computational domain. As cells divide, they push their neighbors and other cells have left the domain at its boundaries. Hence, an adequate boundary condition has to be written for the velocity.

In particular, a compatibility condition has to be satisfied

$$\int_{\partial\Omega} \mathbf{v} \cdot \mathbf{n} = \int_{\Omega} P_2(a_{\max}), \tag{9}$$

where $\mathbf{n}$ denotes the normal at the boundary of the domain Ω.

We decompose the velocity as $\mathbf{v} = \mathbf{w} - \nabla\psi$, where $\mathbf{w} \cdot \mathbf{n} = 0$ and $\psi = 0$ on $\partial\Omega$. Then the function ψ satisfies

$$\begin{cases} \Delta\psi = -P_2(a_{\max}), \\ \psi = 0 \text{ on } \partial\Omega. \end{cases} \tag{10}$$

On the boundaries of the domain, we have $\mathbf{v} \cdot \mathbf{n} = -\frac{\partial\psi}{\partial\mathbf{n}}$, which is known through Eq. (10). As for the tangential component of the velocity $\mathbf{v} \cdot \tau$, we choose to write a Neumann condition:

$$\partial_n (\mathbf{v} \cdot \tau) = 0 \text{ on } \partial\Omega. \tag{11}$$

2.5 Membrane

We wish to take into account the elastic force on the fluid that a membrane produces. This force acts as a source term in the Stokes equations [9]. Note that the width of the membrane is neglected relatively to the tumor size.

2.5.1 Localization

Many methods are available for describing the motion of a membrane. Among these methods, we can cite: the Volume-of-Fluid methods, particles methods and level set methods. We choose to use a level set formulation [8] for its accuracy and because it is easy to implement.

The interface at time t, Γ_t is considered as the zero level set of a function denoted by $\phi(t)$ and moves with the velocity $\mathbf{v}$. More precisely,

$$\Gamma_t = \{\mathbf{x} \in \Omega,\, \phi(t, \mathbf{x}) = 0\}\,. \tag{12}$$

If the interface forms a closed curve, we assume that inside the interface, we have $\phi(t, .) > 0$ and $\phi(t, .) < 0$ outside.

The evolution of the level set function is given by the following equation

$$\partial_t \phi + \mathbf{v} \cdot \nabla \phi = 0, \tag{13}$$

where the initial datum is the signed distance to the interface (*i.e.* $\phi(0, \mathbf{x}) = d(\mathbf{x}, \Gamma_0)$) at the beginning of the simulation.

2.5.2 Degradation

The membrane is also degraded by the tumor cells. At time t, the degradation of a point (x, y, z) of the membrane will be described by the variable $\eta(t, \mathbf{x})$, whose values range from 0 to 1 according to the degradation ($\eta = 0$ meaning there is no longer a membrane at the point considered). While the degradation state η is only defined on Γ_t, we will extend it to the whole domain along the normals to Γ_t. Later on, we will show how to do it numerically.

The variable η evolves through

$$\begin{aligned} &\partial_t \eta + \mathbf{v} \cdot \nabla \eta = -\beta(\mathcal{M}), \\ &\partial_t \mathcal{M} - \nabla \cdot (K_{\mathcal{M}} \nabla \mathcal{M}) = \eta^+ \cdot \textstyle\int_a (P_1 + P_2) - \alpha_{\mathcal{M}}, \end{aligned} \tag{14}$$

where the hyperbolic function β is described in the appendix A and $K_{\mathcal{M}}$ is a coefficient of diffusion. Physically, the quantity $\mathcal{M}$ corresponds to the density of metalloproteinases enzymes produced by the tumor in the vicinity of the membrane. These enzymes attack the membrane and are also degraded by the organism at a rate denoted by $\alpha_{\mathcal{M}}$.

2.5.3 Elasticity

We shall now compute the elastic force from η and ϕ. We consider a two-dimensional membrane in a three-dimensional flow, we mainly follows the approach of [9]. The elastic energy of the membrane is given by

$$\mathcal{E}(t) = \int_{\Gamma_t} \eta^+(\sigma) E(\mathcal{T}(\sigma)) d\sigma,$$

where the elementary energy E is obtained from:

$$E(\mathcal{T}) = T_0(\mathcal{T} - 1), \tag{15}$$

and $\mathcal{T}(\sigma)$ is the stretching factor of the surface at σ.

To obtain the elastic force $\mathbf{F}$, one uses the relation

$$\frac{d}{dt}\mathcal{E}(t) = -\int_{\Gamma_t} \mathbf{F} \cdot \mathbf{v}. \tag{16}$$

Given $\epsilon > 0$, let us define $\Delta_0 = \{\mathbf{x} \in \Omega : |\phi(0, \mathbf{x})| \leq \epsilon\}$ and $\Delta_t = \{\mathbf{x} \in \Omega : |\phi(t, \mathbf{x})| \leq \epsilon\}$. Denote by $\mathbf{X}(t, \xi_1, \xi_2, \xi_3)$ a parametrization of Δ_t such that $\mathbf{X}(0, \xi_1, \xi_2, 0) = \Gamma_0$, $|\partial_{\xi_i}\mathbf{X}(0, \xi)| = 1$, $i = 1, 2, 3$, $\partial_i\mathbf{X}(t, \xi) \cdot \partial_j\mathbf{X}(t, \xi) = 0$ if $i \neq j$ and

$$\partial_t\mathbf{X}(t, \xi) = \mathbf{v}(t, \mathbf{X}(t, \xi)). \tag{17}$$

For the sake of simplicity, we write $\mathbf{X}_{\xi_i}$ for $\partial_{\xi_i}\mathbf{X}$ from now on.

We have $\partial_t[\phi(t, \mathbf{X}(t, \xi))] = [\partial_t\phi](t, \mathbf{X}) + \nabla\phi(t, \mathbf{X}) \cdot \mathbf{v}(t, \mathbf{X}) = 0$ from Eq. (13) and (17). Hence $\phi(t, \mathbf{X}(t, \xi_1, \xi_2, 0)) = \phi(0, \mathbf{X}(0, \xi_1, \xi_2, 0)) = 0$. The surface Γ_t is parametrized by $(\xi_1, \xi_2) \mapsto \mathbf{X}(t, \xi_1, \xi_2, 0)$.

The stretching of the membrane Γ_t at $\mathbf{X}(t, \xi)$ is given by

$$\mathcal{T}(\mathbf{X}) = |\mathbf{X}_{\xi_1} \times \mathbf{X}_{\xi_2}|. \tag{18}$$

In order to compute the elastic force on the tumor due to the membrane, this stretching has to be obtained from ϕ and η.

We define the jacobian J on Δ_t by

$$J(t,\xi_1,\xi_2,\xi_3) = \det(\mathbf{X}_{\xi_1}, \mathbf{X}_{\xi_2}, \mathbf{X}_{\xi_3}). \tag{19}$$

The jacobian evolves according to the equation

$$\partial_t J + \mathbf{v}\cdot\nabla J = (\nabla\cdot\mathbf{v})\, J. \tag{20}$$

We will now prove that $|\mathbf{X}_{\xi_1}\times\mathbf{X}_{\xi_2}|(t,\xi) = (J|\nabla\phi|)(t,\mathbf{X}(t,\xi))$. Indeed, we have

$$\partial_t(\mathbf{X}_{\xi_1}\times\mathbf{X}_{x_2}) = d(\mathbf{v})\mathbf{X}_{\xi_1}\times\mathbf{X}_{x_2} + \mathbf{X}_{\xi_1}\times d(\mathbf{v})\mathbf{X}_{\xi_2}, \tag{21}$$

using equation (17). We have denoted the tensor $[\partial_j v_i]_{i,j}$ by $d(\mathbf{v})$.

The matrix $d(\mathbf{v})$ can be decomposed into $d(\mathbf{v}) = \frac{\operatorname{tr} d(\mathbf{v})}{3}\mathrm{Id} + S + A$, where S is symmetric with a vanishing trace and A is antisymetric (adapting the proof used in [9]). We also know that $\operatorname{tr} d(\mathbf{v}) = \nabla\cdot\mathbf{v}$. Eq. (21) yields:

$$\begin{aligned}\partial_t(\mathbf{X}_{\xi_1}\times\mathbf{X}_{x_2}) &= -S(\mathbf{X}_{\xi_1}\times\mathbf{X}_{x_2}) + A(\mathbf{X}_{\xi_1}\times\mathbf{X}_{x_2}) + \frac{2}{3}\operatorname{tr} d(\mathbf{v})\mathbf{X}_{\xi_1}\times\mathbf{X}_{x_2}\\ &= -[d(\mathbf{v})]^t(\mathbf{X}_{\xi_1}\times\mathbf{X}_{x_2}) + \operatorname{tr} d(\mathbf{v})\mathbf{X}_{\xi_1}\times\mathbf{X}_{x_2}.\end{aligned}$$

With (13) and (20), we can also write:

$$\begin{aligned}\partial_t(J(t,\mathbf{X})\nabla\phi(t,\mathbf{X})) &= \partial_t J(t,\mathbf{X})\nabla\phi(t,\mathbf{X}) - J(t,\mathbf{X})[d(\mathbf{v})]^t\nabla\phi(t,\mathbf{X})\\ &= (\nabla\cdot\mathbf{v})J(t,\mathbf{X})\nabla\phi(t,\mathbf{X}) - J(t,\mathbf{X})[d(\mathbf{v})]^t\nabla\phi(t,\mathbf{X}).\end{aligned}$$

Initialy, we have $\mathbf{X}_{\xi_1}(0,\xi_1,\xi_2,0)\times\mathbf{X}_{x_2}(0,\xi_1,\xi_2,0) = [J\nabla\phi](\mathbf{X}(0,\xi_1,\xi_2,0))$ which completes the proof.

At this stage, our expression for the elastic force is:

$$\mathcal{E}(t) = \int_{\Gamma_t} \eta^+(t,\mathbf{X}) E\left(J(t,\mathbf{X})|\nabla\phi(t,\mathbf{X})|\right) d\xi_1 d\xi_2. \tag{22}$$

Then, we perform the change of variables $\mathbf{x}(t) = \mathbf{X}(t,\xi_1,\xi_2,0)$. The expression of the elastic force in Eulerian variables is:

$$\mathcal{E}(t) = \int_{\Gamma_t} \eta^+(t,\mathbf{x}) E\left(J(t,\mathbf{x})|\nabla\phi(t,\mathbf{x})|\right) J^{-1}(t,\mathbf{x}) d\mathbf{x}.$$

As in [9], the energy is smoothed (on a scale $\epsilon << 1$), which yields the expression $\mathcal{E}_\epsilon$ depending on ϕ, η and J :

$$\mathcal{E}_\epsilon(t) = \int_\Omega E(|\nabla\phi(t,\mathbf{x})|J(t,\mathbf{x}))\frac{1}{\epsilon}\zeta(\frac{\phi(t,\mathbf{x})}{\epsilon})\eta^+(t,\mathbf{x})J^{-1}(t,\mathbf{x})d\mathbf{x}, \tag{23}$$

the term $\frac{1}{\epsilon}\zeta(\frac{\phi(t,x)}{\epsilon})$ being an approximation of the Dirac mass on Γ_t. Practically, we take $\epsilon = 2\delta$, where δ is the typical spatial step.

The smoothing function ζ is classically defined by:

$$\zeta(y) = \begin{cases} \frac{1}{2}(1+\cos \pi y) \text{ if } |y| < 1, \\ 0 \qquad\qquad\qquad \text{otherwise.} \end{cases}$$

To recover the elastic force (through Eq. (16)), we differentiate (23) w.r.t. the time variable t and get,

$$\begin{aligned}\frac{d}{dt}\mathcal{E}_\epsilon(t) = &\int_\Omega \left(E(|\nabla\phi|J)\frac{1}{\epsilon^2}\zeta'(\frac{\phi}{\epsilon})\partial_t\phi\,\eta^+ J^{-1} + E(|\nabla\phi|J)\frac{1}{\epsilon}\zeta(\frac{\phi}{\epsilon})\partial_t\eta^+ J^{-1}\right) d\mathbf{x} \\ &+ \int_\Omega \left(E'(|\nabla\phi|J)\partial_t(|\nabla\phi|J)\frac{1}{\epsilon}\zeta(\frac{\phi}{\epsilon})\eta^+ J^{-1} - E(|\nabla\phi|J)\frac{1}{\epsilon}\zeta(\frac{\phi}{\epsilon})\eta^+\frac{\partial_t J}{J^2}\right) d\mathbf{x},\end{aligned}$$

where

$$\partial_t(|\nabla\phi|J) = \left(\frac{\nabla\phi}{|\nabla\phi|}\cdot\nabla(\partial_t\phi)\right)J + |\nabla\phi|\partial_t J.$$

Furthermore, we know that ϕ is the solution to the advection equation $\partial_t\phi + \mathbf{v}\cdot\nabla\phi = 0$ and that J satisfies $\partial_t J + \mathbf{v}\cdot\nabla J = (\nabla\cdot\mathbf{v})J$.

We shall also compute the term $\partial_t\eta^+$, where wer remind that η is a solution of Eq. (14). To perform an identification with (16), one has to neglect the right-hand side of (14). We multiply this equation by $\mathbf{1}_{\{\eta>0\}}$ to get $\partial_t\eta^+ = -\mathbf{v}\cdot\nabla\eta^+$.

We replace $\partial_t\phi$, $\partial_t\eta^+$ and $\partial_t J$ by their expressions in the former equations and we obtain:

$$\begin{aligned}\frac{d}{dt}\mathcal{E}_\epsilon(t) = &\int_\Omega E(|\nabla\phi|J)\frac{1}{\epsilon^2}\zeta'(\frac{\phi}{\epsilon})(-\mathbf{v}\cdot\nabla\phi)\eta^+ J^{-1} + E(|\nabla\phi|J)\frac{1}{\epsilon}\zeta(\frac{\phi}{\epsilon})(-\mathbf{v}\cdot\nabla\eta^+)J^{-1}\; d\mathbf{x} \\ &+ \int_\Omega E'(|\nabla\phi|J)\left(\frac{\nabla\phi}{|\nabla\phi|}\cdot\nabla(-\mathbf{v}\cdot\nabla\phi)\right)\frac{1}{\epsilon}\zeta(\frac{\phi}{\epsilon})\eta^+\; d\mathbf{x} \qquad (24) \\ &+ \int_\Omega E'(|\nabla\phi|J)|\nabla\phi|\frac{1}{\epsilon}\zeta(\frac{\phi}{\epsilon})\eta^+\left(\nabla\cdot\mathbf{v} - \frac{\nabla J}{J}\cdot\mathbf{v}\right)d\mathbf{x} \qquad (25) \\ &+ \int_\Omega E(|\nabla\phi|J)\frac{1}{\epsilon}\zeta(\frac{\phi}{\epsilon})\eta^+\left(\frac{\nabla J}{J^2}\cdot\mathbf{v} - J^{-1}\nabla\cdot\mathbf{v}\right)d\mathbf{x}. \qquad (26)\end{aligned}$$

Remark 2 *In [9], this expression can be further simplified as $\nabla\cdot\mathbf{v} = 0$. In our case, this equation is no longer satisfied by $\mathbf{v}$ as shown in Eq. (6).*

To simplify the equations we will note $\mathbf{n}_\phi = \frac{\nabla\phi}{|\nabla\phi|}$ and $\mathbf{n}_J = \frac{\nabla J}{J}$.

Let us assume that the velocity $\mathbf{v}$ (of the membrane) is vanishing at the boundary of the domain Ω. This will be enforced numerically. After integrating by parts, line (24) yields:

$$\int_\Omega E'(|\nabla\phi|J)\left(\mathbf{n}_\phi\cdot\nabla(-\mathbf{v}\cdot\nabla\phi)\right)\frac{1}{\epsilon}\zeta(\frac{\phi}{\epsilon})\eta^+\,d\mathbf{x} = \int_\Omega \frac{T_0}{\epsilon}\left(\eta^+\frac{1}{\epsilon}\zeta'(\frac{\phi}{\epsilon})|\nabla\phi| \right.$$
$$\left. +\zeta(\frac{\phi}{\epsilon})(\nabla\eta^+\cdot\mathbf{n}_\phi)+\zeta(\frac{\phi}{\epsilon})\eta^+\kappa_\phi\right)\nabla\phi\cdot\mathbf{v}d\mathbf{x},$$

since, from Eq. (15), $E'(|\nabla\phi|J) = T_0$. We have denoted by $\kappa_\phi = \nabla\cdot\mathbf{n}_\phi$, the curvature of the interface.

The remaining terms in $\nabla\cdot\mathbf{v}$ of (25) and (26) can written:

$$\int_\Omega\left(T_0|\nabla\phi|\frac{1}{\epsilon}\zeta(\frac{\phi}{\epsilon})\eta^+ - E(|\nabla\phi|J)\frac{1}{\epsilon}\zeta(\frac{\phi}{\epsilon})\eta^+J^{-1}\right)\nabla\cdot\mathbf{v}\,d\mathbf{x} = \int_\Omega T_0J^{-1}\frac{1}{\epsilon}\zeta(\frac{\phi}{\epsilon})\eta^+\nabla\cdot\mathbf{v}\,d\mathbf{x},$$

as $T_0J|\nabla\phi| - E(J|\nabla\phi|) = T_0$ thanks to the expression of the elementary energy E from Eq. (15). We integrate by parts,

$$\int_\Omega\frac{T_0}{\epsilon}J^{-1}\zeta(\frac{\phi}{\epsilon})\eta^+\nabla\cdot\mathbf{v}\,d\mathbf{x} = -\int_\Omega\frac{T_0}{\epsilon^2}\zeta'(\frac{\phi}{\epsilon})J^{-1}\eta^+\nabla\phi\cdot\mathbf{v}\,d\mathbf{x} - \int_\Omega\frac{T_0}{\epsilon}J^{-1}\zeta(\frac{\phi}{\epsilon})\nabla\eta^+\cdot\mathbf{v}\,d\mathbf{x}$$
$$+\int_\Omega\frac{T_0}{\epsilon}J^{-1}\zeta(\frac{\phi}{\epsilon})\eta^+\mathbf{n}_J\cdot\mathbf{v}\,d\mathbf{x}.$$

Collecting the above equations, we get:

$$\frac{d}{dt}\mathcal{E}_\epsilon(t) = \int_\Omega\frac{T_0}{\epsilon}\left(\nabla\eta^+\cdot\mathbf{n}_\phi+\eta^+\kappa_\phi\right)\zeta(\frac{\phi}{\epsilon})\nabla\phi\cdot\mathbf{v}\,d\mathbf{x}$$
$$-\int_\Omega\frac{1}{\epsilon}(E(J|\nabla\phi|)+T_0)\zeta(\frac{\phi}{\epsilon})J^{-1}\nabla\eta^+\cdot\mathbf{v}\,d\mathbf{x}$$

Remark 3 *Thanks to the expression of the elementary energy (15), the term along $\mathbf{n}_J$ is vanishing.*

We will see in section 3.4 how to extend the variable η as a constant along the normals to the interface. Hence, we can safely assume that $\nabla\eta^+\cdot\mathbf{n}_\phi = 0$ in the former expression for the elastic force. The identification is straightforward, and we obtain an expression of the elastic force $\mathbf{F}$:

$$\mathbf{F} = -\frac{T_0}{\epsilon}\eta^+\kappa_\phi\zeta(\frac{\phi}{\epsilon})\nabla\phi+\frac{1}{\epsilon}(E(J|\nabla\phi|)+T_0)\zeta(\frac{\phi}{\epsilon})J^{-1}\nabla\eta^+. \tag{27}$$

Remark 4 *The term along $\nabla\phi$ in Eq. (27) is normal to the interface, while the last one is in the transverse direction.*

2.6 Summary of the equations to be solved

We compute the tumoral densities in the proliferating (P_1 and P_2) and quiescent (Q) phases with:

$$\begin{cases} \partial_t P_1 + \partial_a P_1 + \nabla \cdot (\mathbf{v}\, P_1) = 0, \\ \partial_t P_2 + \partial_a P_2 + \nabla \cdot (\mathbf{v}\, P_2) = 0, \\ \partial_t Q + \nabla \cdot (\mathbf{v}\, Q) = (1-f) P_1(a = a_{\max,P_1}) - \left[\frac{d}{dt} f\right]^+ Q(t^-), \\ P_1(a=0) = 2P_2(a = a_{\max,P_2}), \\ P_2(a=0) = f\, P_1(a = a_{\max,P_1}) + \left[\frac{d}{dt} f\right]^+ Q(t^-). \end{cases}$$

The oxygen concentration C evolves through:

$$\begin{cases} -\nabla \cdot (K \nabla C) = -\alpha \sum_{i=1,2} \int_0^{a_{\max,P_i}} P_i(a) da, \\ C = C_0 \ \text{ on } \ \partial\Omega, \\ C = C_{\max} \ \text{ on } \ \mathrm{O}. \end{cases}$$

The velocity of the motion created by the cellular division is computed (along with a potential P) with the following equations:

$$\begin{cases} -\nabla \cdot (\nu D(\mathbf{v})) + \nabla \left(P + \frac{2}{d} \nu \mathrm{tr}(D(\mathbf{v})) \right) = \mathbf{F}, \\ \nabla \cdot \mathbf{v} = P_2(a_{\max,P_2}), \\ \mathbf{v} \cdot \mathbf{n} = -\frac{\partial \psi}{\partial \mathbf{n}}, \partial_n \mathbf{v} \cdot \tau = 0 \text{ on } \partial\Omega, \\ \mathbf{F} = -\frac{T_0}{\epsilon} \eta^+ \kappa_\phi \zeta(\frac{\phi}{\epsilon}) \nabla\phi + \frac{1}{\epsilon}(E(J|\nabla\phi|) + T_0) \zeta(\frac{\phi}{\epsilon}) J^{-1} \nabla \eta^+, \end{cases}$$

where the function ψ satisfies:

$$\begin{cases} \Delta\psi = -P_2(a_{\max,P_2}), \\ \psi = 0, \ \text{on } \partial\Omega. \end{cases}$$

The localization (ϕ), jacobian (J) and state of degradation (η) of the mem-

brane obey:

$$\begin{cases} \partial_t \phi + \mathbf{v} \cdot \nabla \phi = 0, \\ \partial_t J + \mathbf{v} \cdot \nabla J = (\nabla \cdot \mathbf{v}) J, \\ \partial_t \eta + \mathbf{v} \cdot \nabla \eta = -\beta(\mathcal{M}), \\ \partial_t \mathcal{M} - \nabla \cdot (K_{\mathcal{M}} \nabla \mathcal{M}) = \eta^+ \cdot \sum_{i=1,2} \int_0^{a_{\max,P_i}} P_i(a) da - \alpha_{\mathcal{M}} \end{cases}$$

3 Numerical schemes

We have used a finite-volume scheme to discretize our equations. In this classical scheme [15], all the variables but the velocity are evaluated at the center of the numerical cells (squares for a 2D scheme, cubes for a 3D scheme).

Let us first introduce the notations. The quantities to be computed depend on three or four variables: the time t and the space variables x, y and z (in the three-dimensional case).

For a function u defined on the grid, we write $u^n_{i,j,k}$ for the average value of u on the cell centered at the grid point (t_n, x_i, y_j, z_k) where $t_n = n\,\delta t$, $x_i = i\,\delta x$, $y_j = j\,\delta y$, $z_k = k\,\delta z$, δt being the time step, δx, δy, δz the spatial steps.

The scheme, we have used is shown in Figure 3. For convenience, we have only represented the bidimensional scheme but the extension to three dimensions is straightforward.

Fig. 3. A cell in the MAC scheme used in the bidimensional case.

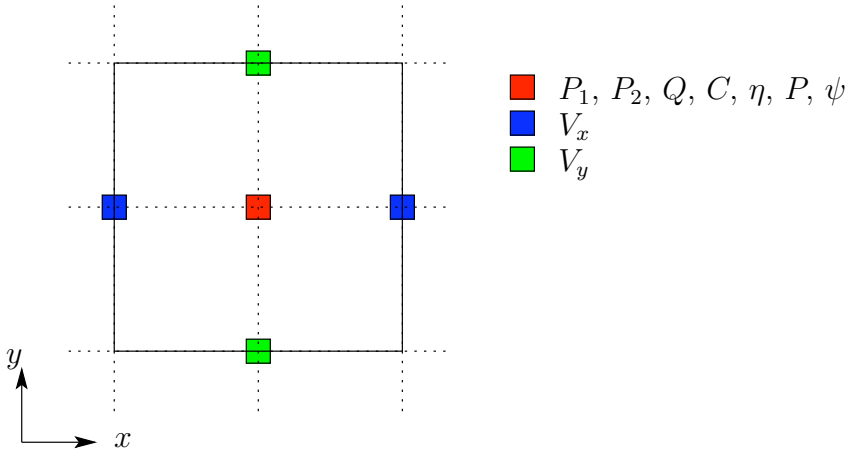

3.1 Diffusion equation

The evolution of the oxygen distribution is solved by successive solution of an elliptic boundary-value problem (7). A penalization method is used to fix the oxygen concentration on the part O of the domain. This means that one solves

$$-\nabla \cdot (K \nabla C) + \frac{1}{\varepsilon}(C - C_{\max})\mathbf{1}_O = -\alpha \sum_{i=1,2} \int_0^{a_{\max,P_i}} P_i(a) da, \qquad (28)$$

for ε small enough (in practice $\varepsilon = 10^{-10}$).

We integrate Eq. (28) over one cell and apply the Stokes theorem. This yields a linear system, that we have to solve at each time step. For this purpose, we use an iterative method [16,17].

To ensure continuity of the flux, the diffusion coefficient at the boundaries of the cell is not computed by linear interpolation.

For instance, in the bidimensional case, to obtain the equation on $C^{n+1}_{i+\frac{1}{2},j+\frac{1}{2}}$ (see Figure 3), we need the values $K^{n+1}_{i,j+\frac{1}{2}}$, $K^{n+1}_{i+1,j+\frac{1}{2}}$, $K^{n+1}_{i+\frac{1}{2},j}$ and $K^{n+1}_{i+\frac{1}{2},j+1}$.

According to Appendix A, the diffusion coefficient can be obtained in the center of the cells by:

$$K^{n+1}_{i+\frac{1}{2},j+\frac{1}{2}} \sim D_{\text{ext}} \left(\sum_a ([P_1 + P_2]^n_{i+\frac{1}{2},j+\frac{1}{2}}) + Q^n_{i+\frac{1}{2},j+\frac{1}{2}} \right) - [\eta^+]^n_{i+\frac{1}{2},j+\frac{1}{2}},$$

the function D_{ext} being described in appendix A.

Then, we approximate $K^{n+1}_{i,j+\frac{1}{2}}$ by $\frac{2K^{n+1}_{i+\frac{1}{2},j+\frac{1}{2}} K^{n+1}_{i-\frac{1}{2},j+\frac{1}{2}}}{K^{n+1}_{i+\frac{1}{2},j+\frac{1}{2}} + K^{n+1}_{i-\frac{1}{2},j+\frac{1}{2}}}$ instead of $\frac{K^{n+1}_{i+\frac{1}{2},j+\frac{1}{2}} + K^{n+1}_{i-\frac{1}{2},j+\frac{1}{2}}}{2}$ and use similar approximations for the remaining values.

3.2 Advection equations and densities evolution

To compute the elastic force, we have to compute second-order derivatives of the level set function ϕ as shown in Eq. (27) for instance. Hence, to have a consistent approximation of these derivatives, we need at least a second order scheme for discretizing the advection equation on the level set function.

To discretize the various advection equations (on cell densities, level set function,...), we use a fifth-order WENO discretization in space and a third-order Runge-Kutta scheme in time [18].

In the following, we recall briefly the principle of WENO schemes. The spatial derivatives have to be computed at the cells center (as the variable we wish to transport). To avoid large numerical diffusion, we need an high-order scheme to approximate the spatial derivative. To prevent instabilities, we also have to avoid areas where the advected quantity is discontinuous. In the fifth-order WENO scheme, the numerical flux at the cell boundaries are computed as a convex combination of three 3-points stencils where each stencil is weighted according to the regularity of the function on this stencil. We will denote by L the discrete operator corresponding to the spatial discretization these advection equations using a WENO scheme.

To prevent temporal oscillations to occur, we use a third-order Runge-Kutta scheme. The advected quantity ϕ^{n+1} at time $t = (n+1)\delta t$ is obtained from the previous value (ϕ^n) in three steps:

$$\begin{cases} \phi^{(1)} &= \phi^n + \delta t L(\phi^n), \\ \phi^{(2)} &= \frac{3}{4}\phi^n + \frac{1}{4}\phi^{(1)} + \frac{1}{4}\delta t L(\phi^{(1)}), \\ \phi^{n+1} &= \frac{1}{3}\phi^n + \frac{2}{3}\phi^{(2)} + \frac{2}{3}\delta t L(\phi^{(2)}). \end{cases} \tag{29}$$

The time step δt is computed at every iteration to ensure that the CFL conditions holds through:

$$\delta t = c_{\mathrm{CFL}} \min\left(\frac{\delta x}{|v_x|_\infty}, \frac{\delta y}{|v_y|_\infty}, \frac{\delta z}{|v_z|_\infty}\right), \tag{30}$$

where we take $c_{\mathrm{CFL}} = 0.45$ in the following.

Thanks to this accurate scheme for the advection equation, we can derive a numerical scheme for the equations leading the evolution of the cellular densities.

Let us denote by ψ, the density in a particular phase ψ (namely P_1 or P_2). The equation on ψ is written as:

$$\partial_t \psi + \partial_a \psi + \mathbf{v} \cdot \nabla \psi + (\nabla \cdot \mathbf{v})\psi = 0.$$

Using a splitting method, we solve this equation with three steps.

In the first step , we solve $\partial_t \psi + \partial_a \psi = 0$ with an first-order upwind scheme. We use an optimal time step ($\delta t = \delta a$) since the velocity in age a is constant.

Next, for the equation $\partial_t \psi + \mathbf{v} \cdot \nabla \psi = 0$, we use the numerical scheme for the advection equations, we have just described.

Finally, we can solve $\partial_t \psi + (\nabla \cdot \mathbf{v})\psi = 0$ explicitly. Let us recall that $\nabla \cdot \mathbf{v} = P_2(a_{\max,P_2})$. We have $\psi^{n+1} = \exp(-P_2^n(a_{\max,P_2})\delta t)\psi^n$.

In equation (14) describing the evolution of the state of the membrane, the right-hand is evaluated at the previous time step that is to say that at time $t_{n+\frac{1}{2}}$, we take $[\beta(\eta^+ \cdot \sum_a (P_1 + P_2))]^{n+\frac{1}{2}} \sim \beta([\eta^+]^n \cdot \sum_a [P_1 + P_2]^n))$.

3.3 Stokes equation

To compute the velocity and pressure of the fluid, we have to solve the Stokes equations. The main difficulty is to ensure that the divergence of the velocity satisfies Eq. (6). Many methods have been developed for this problem. For instance, one can see [19,20]. In order to ensure that we have a correct value for this divergence, we use the method the augmented Lagrangian method, see Fortin and Glowinski [21].

With this method, velocity and pressure are no longer coupled. Boundary conditions are not needed for the pressure term. The principle is to add a pressure term to Eq. (8),

$$\begin{cases} -\nabla \cdot (\nu D(\mathbf{v})) + \nabla P = \mathbf{F} \\ \\ \epsilon_0 \partial_r P + \nabla \cdot \mathbf{v} = \sigma, \end{cases} \tag{31}$$

where $\sigma = P_2(a_{\max,P_2})$.

In Eq. (31), we have replaced the pressure P by $P + \frac{2}{d}\nu \mathrm{tr}(D(\mathbf{v}))$. Indeed, we have

$$\mathrm{tr}(D(\mathbf{v})) = \nabla \cdot \mathbf{v} = P_2(a_{\max}). \tag{32}$$

The stationary solution to (31), is the solution to the Stokes equations (8). Between two time steps, we will perform L Lagrangian iterations to approximate the stationary solution of Eq. (31).

Eq. (31) is discretized in time, (Augmented Lagrangian steps are denoted by fractional time steps):

$$\begin{cases} -\nabla \cdot (\nu D(\mathbf{v}^{n+\frac{\ell}{L}})) + \nabla P^{n+\frac{\ell}{L}} = \mathbf{F}^n, \quad 1 \leq \ell \leq L, \\ \\ P^{n+\frac{\ell}{L}} - P^{n+\frac{\ell-1}{L}} = -r\nabla \cdot v^{n+\frac{\ell}{L}} + r\sigma^n, \end{cases} \tag{33}$$

where $r = \frac{dr}{\epsilon_0}$. In our computations, we took $r = 2$. We replace $P^{n+\frac{\ell}{L}}$ in the first equation by its expression obtained from the second one. Thus we get a

new system, where velocity and pressure are no longer coupled:

$$\begin{cases} -\nabla \cdot (\nu D(\mathbf{v}^{n+\frac{\ell}{L}})) - r\nabla(\nabla \cdot \mathbf{v}^{n+\frac{\ell}{L}}) = -\nabla P^{n+\frac{\ell-1}{L}} + \mathbf{F}^n - r\nabla\sigma^n, \quad 1 \leq \ell \leq L, \\ P^{n+\frac{\ell}{L}} = P^{n+\frac{\ell-1}{L}} - r\nabla \cdot v^{n+\frac{\ell}{L}} + r\sigma^n. \end{cases} \tag{34}$$

Each equation of system (34) is written on a different cell. The second equation giving the pressure term $P^{n+\frac{\ell}{L}}$ is written on the cell centered on P. For the velocity components, we use staggered grids shifted by half a spatial step in the direction of the velocity component we wish to compute.

Thus, a linear system on the velocity is obtained. This system is solved at every iteration [16,17]. Once the velocity is computed, the pressure is obtained from the last equation of (34).

It remains to estimate the elastic force $\mathbf{F}^n$ appearing as a source term in Eq. (34). We know that this force is vanishing outside the interface. At a given point $\mathbf{x}$ of the domain, we have to compute $\mathbf{F}^n$ only if $|\phi(t_n, \mathbf{x})| < \epsilon$, otherwise $\mathbf{F}^n(\mathbf{x}) = 0$.

First, let us evaluate Eq. (27) at time t_n:

$$\mathbf{F}^n = -\frac{T_0}{\epsilon}[\eta^+]^n \kappa_\phi^n \zeta(\frac{\phi^n}{\epsilon})[\nabla\phi]^n + \frac{1}{\epsilon}(E(J^n|\nabla\phi|^n) + T_0)\zeta(\frac{\phi^n}{\epsilon})\frac{1}{J^n}[\nabla\eta^+]^n. \tag{35}$$

We have to compute $[\nabla\phi]^n$, κ_ϕ^n and $[\nabla\eta^+]^n$. The first-order terms $[\nabla\phi]^n$ and $[\nabla\eta^+]^n$ are obtained through a WENO scheme as in the discretization of the advection equations (13) and (14).

The curvature $\kappa = \nabla \cdot \frac{\nabla\phi}{|\nabla\phi|}$ is computed from $[\nabla\phi]^n$ by a centered discretization.

3.3.1 Boundary conditions

In order to obtain the values of the velocity $\mathbf{v}$ at the boundary of the domain, we have to compute ψ solution of Eq. (10).

First, we compute ψ^{n+1} using the scheme described in section 3.1.

As the computational domain is rectangular, we have $v_x|_{0,j}^{n+1} = -[\partial_x\psi]_{0,j}^{n+1}$, $v_x|_{N_x,j}^{n+1} = -[\partial_x\psi]_{N_x,j}^{n+1}$, $v_y|_{i,0}^{n+1} = -[\partial_y\psi]_{i,0}^{n+1}$ and $v_y|_{i,N_y}^{n+1} = -[\partial_y\psi]_{i,N_y}^{n+1}$.

The spatial derivatives $\partial_x\psi$ and $\partial_y\psi$ are easily computed at the boundary of the domain using a second order approximation and the fact that ψ vanishes at the boundary.

3.4 Redistanciation and renormalization equations

The level set function ϕ evolves through an advection equation (13). Initially, the function ϕ is the signed distance to the interface. Of course for $t > 0$, ϕ is not the distance to the interface anymore. However at each time step, we need to compute the elastic force, we need to detect the zero level set and we need to ensure that the membrane width characterized by $|\phi| < \epsilon$ keeps its physical meaning. All these points are easier to ensure with a function ϕ that is the distance to the interface.

For this purpose, we perform a redistanciation step [8] consisting in resolving an Hamilton-Jacobi equation on the level set ϕ:

$$\partial_\tau \phi + \mathrm{sgn}(\phi_0)\,(|\nabla \phi| - 1) = 0, \tag{36}$$

where ϕ_0 denotes the function ϕ at the beginning of the reinitialization step and sgn the (smoothed) sign function defined by:

$$\mathrm{sgn}(\phi_0)_{ij} = \frac{(\phi_0)_{ij}}{\sqrt{(\phi_0)_{ij}^2 + \delta x^2}}. \tag{37}$$

Let us note that as the sign function is vanishing for the zero level set, this equation does not modify this level set. The stationary solution to Eq. (36) is the signed distance to Γ_t. The principle of the redistanciation process is to replace ϕ by the stationary solution of Eq. (36).

The discretization scheme is based on [22]. The term $\nabla \phi$ is computed using a fifth-order WENO scheme. We then use a Godunov flux, whose expression is simple in the case of (36). The time-integration is performed using a TVD third-order Runge-Kutta scheme [23].

The pseudo time step $\delta\tau$ depend on the spatial step, we choose to take $\delta\tau = \frac{\min(\delta x, \delta y, \delta z)}{10}$ which satisfies the CFL condition for Eq. (36). The reinitialization process starts from the zero level set and progresses toward the normals. Thus, only a few steps of (36) are needed to ensure that the function ϕ is identical to the distance function in the vicinity of the interface. Practically, a rule of thumb is that it requires a number of time steps of the order of the number of grid-points in the support of the smoothing function ζ.

We shall also note that the state of the extra-cellular matrix η is only defined on the zero level of the function ϕ. To compute $\nabla \eta^+$, we extend the variable on a few cells around the interface. We perform this extension along the normals of Γ_t, thus η is constant along the normals (see the point after Remark 3). To this aim, we replace η by an approximation of the stationary solution to the

following equation [24]:

$$\partial_\tau \eta + \mathrm{sgn}(\phi)\frac{\nabla\phi}{|\nabla\phi|}\cdot\nabla\eta = 0, \tag{38}$$

where sgn is defined in Eq. (37). As for the redistanciation equation, we use a WENO scheme to compute the spatial derivatives and a TVD Runge-Kutta scheme for the temporal discretization.

4 Numerical Experiments

To save computational time, we use a sub-cycling method. Indeed, the typical time-scales of all the phenomena are not the same. This is summarized in Table 1.

Table 1
Time scales of the various biological phenomena.

Scale	Phenomenon	Typical value
Cell Cycle	Cellular division	1
Cellular scale	Diffusion – Degradation	$\frac{1}{10}$
Fluid Scale	Stokes – Advection	$\frac{1}{100}$

The various parameters used are listed in Table A.1 of Sec. A. We took the total number of cells per unit volume N_0 (see Eq. (5)) equals to 1.

4.1 Environmental and external conditions

In the following experiments, we use the experimental setup shown in Figure 4. We have plotted the interface with its numerical width ($|\phi| < \epsilon$, while in theory it should be $|\phi| = 0$). The level set function ϕ is initialized to the signed distance to the interface. The ECM is initially not degraded, hence we have $\eta^0_{i+\frac{1}{2},j+\frac{1}{2},k+\frac{1}{2}} = 1$ if $|\phi^0_{i+\frac{1}{2},j+\frac{1}{2},k+\frac{1}{2}}| < \epsilon$ and η^0 is vanishing elsewhere.

The inital tumoral distribution was taken from a scan image (courtesy David Sarrut, Centre Léon Bérard, Lyon, France). Initially, all the tumor cells are uniformly distributed between proliferating phases.

Fig. 4. Experimental setup. The membrane (plotted in white) divides the domain in two parts. The oxygen supply (in green) can be found in the upper part of the domain, while the initial tumor is in the lower part. The color bar describes the tumor cells density.

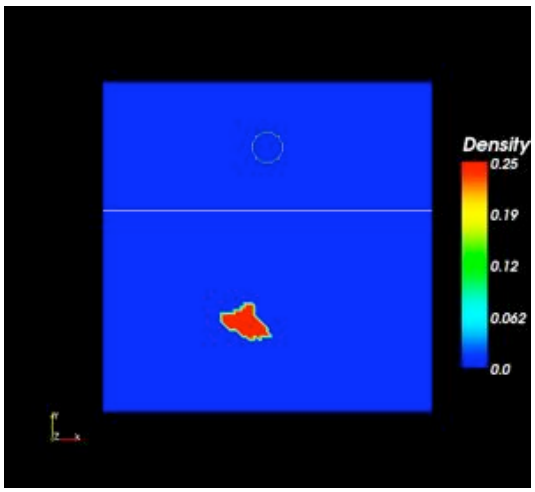

4.1.1 Hypoxia

In this section, we study the effect of the lack of oxygen on the tumor growth. We neglect the overpopulation factor (*i.e.* $\tau_o > N_0$).

The experimental setup is the following. We have taken the threshold of hypoxia $\tau_o = 0.2$. For this run, we have used a 100×100 grid. The spatial step is equal to 0.08 for both dimensions. We use a CFL condition of 0.45. The experiment is run until $T = 120$. To improve computation times, we do not renormalize the level set function ϕ or extend the matrix state η at each time step but only on even iterations. The initial tumor was obtained from a scan image. We have taken $C_{\max} = 10$ in Eq. (7).

In Figure 5, we have plotted the density of total tumoral density and the proliferative density at the end of the experiment.

We observe the growth of the tumor in the direction of the oxygen supply. Indeed, at the beginning of the experiment, the cells undergo mitosis and the tumor is growing. However, as there are more and more proliferating cells, the consumption of oxygen rises thus lowering the concentration. The hypoxia threshold is overpassed and many cells become quiescent.

We observe that far from the oxygen supply, the tumors cells are massively quiescent and do not participate to the tumor growth. In regions with higher oxygen concentration, the tumor is still expanding. The mitotic cells are found in the closest part of the tumor to oxygen well.

Fig. 5. Total and proliferative tumoral density at the end of the experiment. We have shown in green two isolines ($C = 0.2$ and $C = 10$) of the oxygen concentration C.

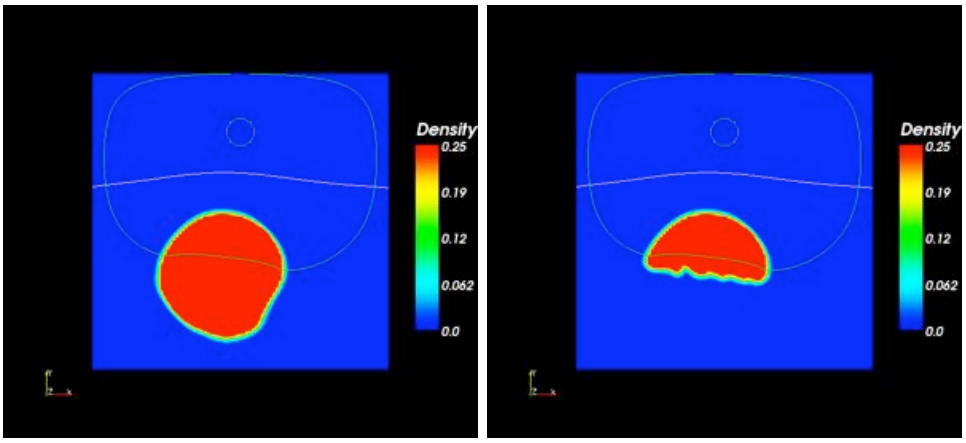

4.1.2 Overpopulation

We will now study the effect of overcrowding on the tumor growth. We do not consider the hypoxia effect, so the hypoxia threshold is vanishing ($\tau_h = 0$). The overpopulation threshold is $\tau_o = 0.5N_0$.

Let us note that, as the hypoxia threshold is vanishing, the growth is isotropic.

We use the same numerical parameters as in the previous experiment.

The total density of tumor cells (in the quiescent and proliferative state) is shown in Figure 6.

Fig. 6. Total and proliferative tumoral density at the end of the experiment.

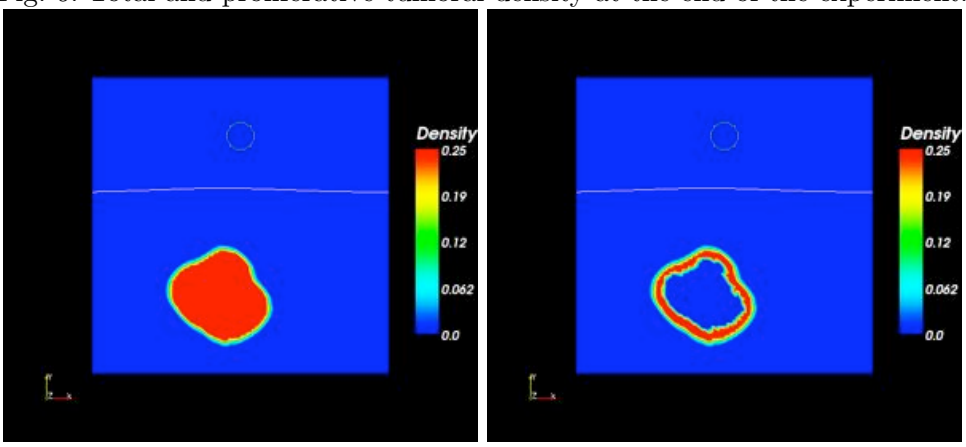

As the tumor grows, it reaches the overpopulation threshold and the cells turns into the quiescent state. Hence, we observe that at the center of the tumor, the density appears to be lower than at its edges. As the overcrowding effect goes, it stops the growth.

At the end of the run, all the tumor cells are in the quiescent state in the center. The overpopulation threshold is not attained by outer cells, the cells are still dividing.

Let us also point out, that the shape of the tumor is completely different from the one observed in the previous section where cells undergo hypoxia.

4.1.3 Elastic force

In this section, we study the effect of the surface tension on the tumor growth. For this purpose, we took two different values of T_0 in Eq. (15), $T_0 = 0.0$ and $T_0 = 0.3$. The experimental conditions are the following. The hypoxia and overpopulation threshold are respectively $\tau_o = 0.75N_0$, $\tau_h = 0.5$. We let the experiment run until $T = 150$. The numerical parameters are the same as in the previous runs (though in this case the initial tumor is centered on the computational domain). The position of the membrane is plotted with a plain white line.

Fig. 7. Density of the cancer cells at the end of the experiment. From left to right, we present the results obtained for $T_0 = 0.0$ and $T_0 = 0.3$. The green line represents the isoline $C = 16$ of the oxygen concentration.

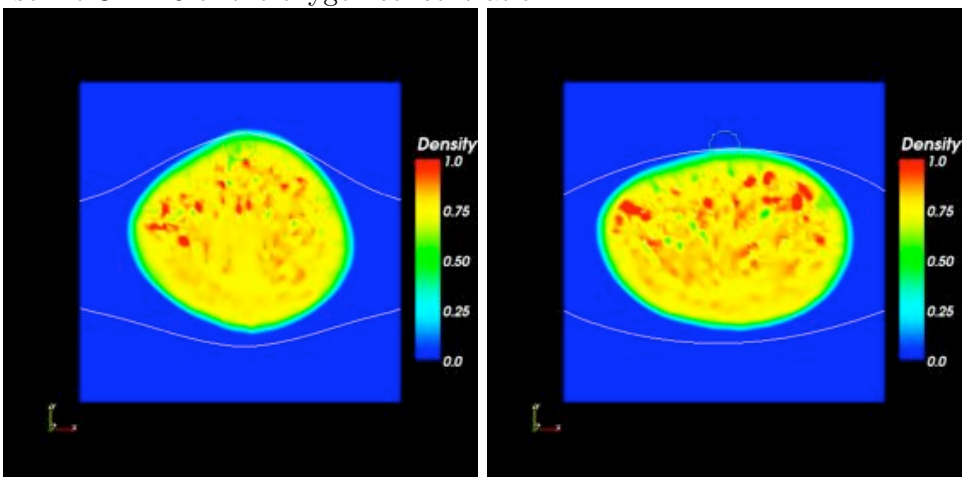

As expected, with a higher tension of the interface, the tumor shape is different. The elastic force limits the tumor expansion in the direction of the oxygen supply. The tumor extends somehow horizontally.

4.2 3D experiments

4.2.1 Porosity of the membrane

In this experiment, we consider a tumor separated from an oxygen supply by a membrane in three dimensions. Depending on this membrane porosity, the concentration of oxygen will vary in the domain where tumor cells stand. Thus, the rate of growth and the shape of the tumor will depend on this porosity.

The porosity of the membrane is modeled by modifying the diffusion coefficient across the interface. In this experiment, we have considered a model with exponential growth (*i.e.* we consider only one mitotic phase, no quiescent phase, no aging and a growth rate depending on the oxygen concentration C). The initial tumor is a sphere separated from the oxygen supply by a membrane, (*i.e.* the 3D extension of the setup shown in Fig. 4). The results are shown on Figure 8.

Fig. 8. Density of the tumor cells at the end of the experiment for two values of the porosity of the membrane. In the rightmost picture, we have considered a lower porosity of the membrane.

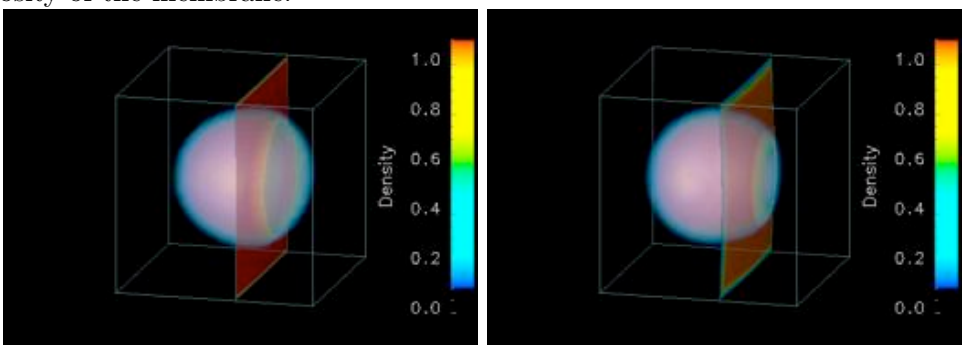

As expected, with a lower porosity, the tumor is smaller as the rate of growth depends on the oxygen distribution.

4.2.2 A complete three-dimensional case

In this section, we study the evolution of a tumor with a three-dimensional scheme with all biological features the model can integrates. This initial tumor is a spheroid. The oxygen is supplied to the tumor by a cylinder where the oxygen concentration is fixed at $C_{\max} = 15$.

We took a $74 \times 74 \times 74$ grid, which yields $\delta x = \delta y = \delta z = 0.0547945$. The tension factor T_0 in Eq. (15) equals 0.01. The two thresholds are respectively $\tau_h = 0.5$, $\tau_o = 0.8 N_0$. We let the experiment run until $T = 150$.

We have shown the density of tumoral cells and the density of quiescent cells

at the end of the run on Figure 9.

Fig. 9. Total and quiescent density of the tumoral cells at the end of the experiment. The oxygen supply is plotted in red.

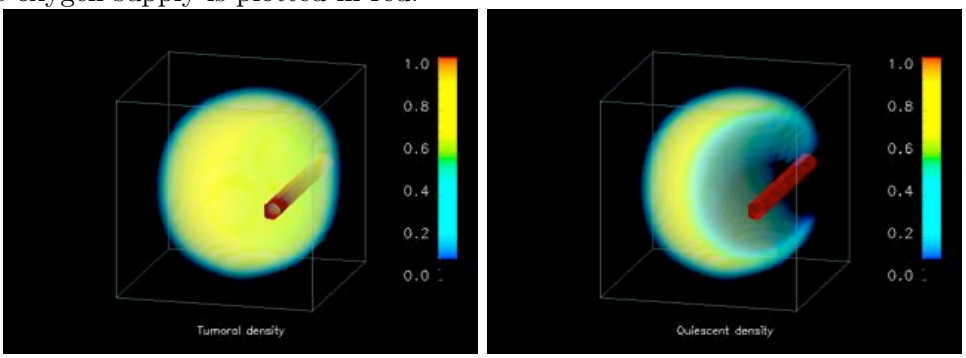

At the end of the experiment, the oxygen supply is surrounded by mitotic cells, while the outer part of the tumor is in the quiescent state.

5 Conclusion

We presented a mathematical and computational model of avascular tumor growth. Respect to existing work, our model describe with more precision both cell cycle regulation and tissue constraints which allow to investigate qualitatively the feedback between macroscopic and microscopic levels.

This model uses a continuous approach through several PDEs based on fluid dynamics. The velocity is obtained from a Stokes equation, where the spatial expansion is translated into a constraint on the divergence of this velocity. The influence of a membrane surrounding the tumor is taken into account as a second hand term in the Stokes equation following the IMB method. Finally, to describe the tumor environment, we use a penalization method in a diffusion equation on the oxygen concentration. We are presently working on a model including tissue elasticity.

On a computational point of view, the model has been implemented with a spirit of modularity rending very easy the implementation of supplement biological phenomena such as, for instance, the role of acidity on cell cycle regulation. In fact, the present work constitutes a computational platform for integrating a maximum of biological knowledge on cancer growth. The significant next step will be to implement the angiogenesis process which will allow us to propose tumor growth models for both avascular and vascular stages.

Acknowledgments

BR has been partially funded by the ETOILE project: "Espace de Traitement Oncologique par Ions Légers dans le cadre Européen".

OS acknowledges stimulating discussions with Pierre Fabrie (Institut de Mathématiques de Bordeaux).

References

[1] D. Hanahan, R. Weinberg, The Hallmarks of Cancer, Cell 100 (1) (2000) 57–70.

[2] R. Bast, D. Kufe, R. Pollock, R. Weichselbaum, J. Holland, Cancer Medicine, BC Decker Inc, Canada, 2000.

[3] B. Alberts, D. Bray, J. Lewis, M. Raff, K. Roberts, J. Watson, Molecular Biology of the Cell, Garland Publishing, New York and London, 1994.

[4] J. Clairambault, B. Laroche, S. Mischler, B. Perthame, A mathematical model of the cell cycle and its control, Rapport de recherche 4892, INRIA (2003).

[5] B. Ribba, T. Colin, S. Schnell, A multiscale mathematical model of cancer, and its use in analyzing irradiation therapies, Theoretical Biology and Medical Modelling 3 (1) (2006) 7.

[6] B. Ribba, O. Saut, T. Colin, D. Bresch, E. Grenier, J. Boissel, A multiscale mathematical model of avascular tumor growth to investigate the therapeutic benefit of anti-invasive agents, J. Theoret. Biol. 243 (4) (2006) 532–541.

[7] C. S. Peskin, The immersed boundary method, Acta Numer. 11 (2002) 479–517.

[8] S. Osher, R. Fedkiw, Level set methods and dynamic implicit surfaces, Vol. 153 of Applied Mathematical Sciences, Springer-Verlag, New York, 2003.

[9] G.-H. Cottet, E. Maitre, A level-set formulation of immersed boundary methods for fluid-structure interaction problems, C. R. Math. Acad. Sci. Paris 338 (7) (2004) 581–586.

[10] M. Blagosklonny, A. Pardee, The restriction point of the cell cycle., Cell Cycle 1 (2) (2002) 103–10.

[11] C. Potten, M. Kellett, S. Roberts, D. Rew, G. Wilson, Measurement of in vivo proliferation in human colorectal mucosa using bromodeoxyuridine, Gut 33 (1) (1992) 71–78.

[12] D. Rew, G. Wilson, I. Taylor, P. Weaver, Proliferation characteristics of human colorectal carcinomas measured in vivo, Br J Surg 78 (1) (1991) 60–6.

[13] D. Ambrosi, L. Preziosi, On the closure of mass balance models for tumor growth, Math. Models Methods Appl. Sci. 12 (5) (2002) 737–754.

[14] G. Bayada, M. Chambat, Conditions aux limites à l'interface d'un milieu poreux et d'un écoulement libre de faible épaisseur, Comptes rendus de l'Académie des sciences. Série 1, Mathématique 315 (4) (1992) 491–495.

[15] S. Patankar, Numerical Heat Transfer and Fluid Flow, Hemisphere Publishing Corporation, 1980.

[16] S. Balay, W. D. Gropp, L. C. McInnes, B. F. Smith, Petsc home page, http://www.mcs.anl.gov/petsc (2001).

[17] S. Balay, W. D. Gropp, L. C. McInnes, B. F. Smith, Petsc users manual, Tech. Rep. ANL-95/11 - Revision 2.1.3, Argonne National Laboratory (2002).

[18] R. P. Fedkiw, B. Merriman, S. Osher, Simplified discretization of systems of hyperbolic conservation laws containing advection equations, J. Comput. Phys. 157 (1) (2000) 302–326.

[19] A. J. Chorin, A numerical method for solving incompressible viscous flow problems [J. Comput. Phys. **2** (1967), no. 1, 12–36], J. Comput. Phys. 135 (2) (1997) 115–125, with an introduction by Gerry Puckett, Commemoration of the 30th anniversary {of J. Comput. Phys.}.

[20] R. Temam, Navier-Stokes equations, revised Edition, Vol. 2 of Studies in Mathematics and its Applications, North-Holland Publishing Co., Amsterdam, 1979, theory and numerical analysis, With an appendix by F. Thomasset.

[21] M. Fortin, R. Glowinski, Méthodes de lagrangien augmenté, Vol. 9 of Méthodes Mathématiques de l'Informatique [Mathematical Methods of Information Science], Gauthier-Villars, Paris, 1982, applications à la résolution numérique de problèmes aux limites. [Applications to the numerical solution of boundary value problems].

[22] G.-S. Jiang, D. Peng, Weighted ENO schemes for Hamilton-Jacobi equations, SIAM J. Sci. Comput. 21 (6) (2000) 2126–2143 (electronic).

[23] S. Gottlieb, C.-W. Shu, Total variation diminishing Runge-Kutta schemes, Math. Comp. 67 (221) (1998) 73–85.

[24] J.-J. Xu, Z. Li, J. Lowengrub, Z. Hongkai, A level-set method for interfacial flows with surfactant, J. Comput. Phys. 212 (2) (2006) 590–616.

A Numerical parameters and functions

The coefficient K leading the diffusion of oxygen in Eq. (7) is obtained from the tumoral density and the position and degradation of the membrane:

$$K(t, \mathbf{x}) = D_{\text{ext}} \left(\sum_a (P_1 + P_2) + Q \right) - \eta^+, \tag{A.1}$$

where the function D_{ext} has the following expression

$$D_{\text{ext}}(z) = \frac{D_0 + D_1}{2} - \frac{D_0 - D_1}{2} \tanh(\frac{z - D_{50}}{D_2}), \tag{A.2}$$

with $D_0 = 5$, $D_1 = 2$, $D_{50} = \frac{1}{2}$ and $D_2 = \frac{1}{20}$. This means that the diffusion coefficient of oxygen is smaller in the tumor than in sane tissue and that the membrane inhibits the diffusion of oxygen.

The function β in (14) is defined as

$$\beta(z) = \beta_{\max} + \beta_{\max} \tanh(20(z - 4)), \tag{A.3}$$

where $\beta_{\max} = 5$.

The viscosity in equation (8) has the following expression:

$$\nu(t, \mathbf{x}) = \frac{2 - \frac{1}{N_0}[Q(t, \mathbf{x}) + \sum_{i=1,2} \int_0^{a_{\max,P_i}} P_i(t, \mathbf{x}) da]}{2},$$

this means that the presence of tumor cells decreases the viscosity. Indeed the cancer cells are more soluble than sane cells.

On Table A.1, we list the various numerical parameters used in our computations.

Table A.1
Numerical parameters used in our computations.

Description	Parameter	Value
Duration of the phase P_1	$a_{\max,P_1}$	10
Duration of the phase P_2	$a_{\max,P_2}$	6
Length of the domain	L_d	8
Width of the domain	D_d	8